NON-LINEAR SPECTROSCOPIC STUDIES
USING SUM- AND DIFFERENCE-FREQUENCY GENERATION [1]

B. DICK [2] and R.M. HOCHSTRASSER

Department of Chemistry, University of Pennsylvania, Philadelphia, Pennsylvania 19104, USA

A detailed study is presented of resonant sum- and difference-frequency generation in the mixed-crystal system azulene in naphthalene. The $S_0 \to S_1$, $S_0 \to S_2$ and $S_1 \to S_2$ transitions of azulene provide the three needed dipoles for the existence of $\chi^{(2)}$, and a relatively small static electric field is used to break the interference between the waves generated in the two crystal sublattices. It is found that second-order non-linear processes can be caused to occur separately in each sublattice. All the theoretically predicted resonances, except the DICE effect, were observed. The generated field intensity was found to saturate at higher fields, and in certain circumstances exhibited hysteresis as a function of the dc-field strength. The line-narrowing capabilities of these new forms of spectroscopy were explored.

1. Introduction

Non-linear coherent effects based on the third-order susceptibility, $\chi^{(3)}$, have found wide application in spectroscopy. Some of the more common examples [1] are CARS, CSRS, polarization spectroscopy, and coherent Rayleigh scattering. The second-order electric susceptibility, $\chi^{(2)}$, has seldom been used in spectroscopic applications because processes determined by it do not occur for isotropic media. However, traditional $\chi^{(2)}$ phenomena such as sum- and difference-frequency generation can be brought about for all media in the presence of dc electric fields. Although the resulting effects are strictly third order in the applied fields, two optical and one dc, the coherent light generation pathways and the dynamical parts of the susceptibility determining the spectral shapes are characteristic of $\chi^{(2)}$ processes. Thus, in addition to the study of non-centrosymmetric systems, $\chi^{(2)}$ spectroscopies can be expected to be applicable also to isotropic media.

Recently several types of $\chi^{(2)}$ resonance were predicted [2] that should allow the determination of interesting and otherwise difficult to measure molecular parameters. For example, there is a $\chi^{(2)}$ analogue of the DICE effect [3–7] that was discovered to occur in CSRS processes under fully resonant conditions. The $\chi^{(2)}$ version occurs in a three-level rather than the usual four-level system of $\chi^{(3)}$ spectroscopy. A study of DICE intensities and lineshapes yields direct information on pure dephasing processes otherwise only available indirectly by separate measurements of T_2 and T_1. We also showed that a number of three-level $\chi^{(2)}$ processes can result in line-narrowed spectra which are useful in high-resolution spectroscopy involving the ground state and also transitions between excited states, in optical hole-burning dynamics, and in yielding novel information on the correlation of the inhomogeneous frequency distributions associated with different transitions. Our preliminary experiments [8] have shown that a number of these predictions can be realized. The purpose of the present paper is to provide a detailed discussion of such pseudo-$\chi^{(2)}$

experiments on the mixed-crystal system azulene in naphthalene. We chose this system because of the extensive existing knowledge of its low-temperature spectroscopy [9–15]; the convenient positioning of its first three electronic states S_0, S_1 and S_2 in relation to the availability and detectability of the three resonant waves that can couple S_0, S_1, and S_2; and the fact that very precise data are available on the effects of electric fields on the azulene resonances [11].

Although a mixed crystal of a polar guest molecule doped in a centrosymmetric host contains dipolar molecules the material is nevertheless non-polar: The substitutional site for the dipole is centrosymmetric so that the average dipole moment of the mixed crystal is zero. In the presence of a dc electric field the random lattice of guest molecules is transformed into two interpenetrating but distinguishable sublattices consisting of polar molecules whose dipoles project parallel and antiparallel to the applied field [16]. The optical transitions of the guest molecules in these two sublattices can then be separately observed, and the splittings can be used to determine the changes of electric dipole moment occurring on excitation. If this system is now subject to an intense electromagnetic field having an arbitrary frequency it will respond as if it were non-centrosymmetric. Conventional electric-field-induced second-harmonic generation will occur, for example, with the SHG radiation intensity depending on the square of the dc-field strength. However a qualitatively different effect is expected if the oscillating field is nearly resonant with one of the guest transitions corresponding to just one of the polar sublattices. In this case the field senses a material which is polar, and at sufficiently high dc fields the $\chi^{(2)}$ processes, occurring as a result of the response of one sublattice, should be nearly independent of dc-field strength. In the present paper the polar molecule is azulene and the non-polar host is naphthalene. The experiments are carried out with optical fields chosen to be resonant with spectrally sharp vibronic transitions of the $S_0 \rightarrow S_1$ and $S_0 \rightarrow S_2$ transitions of azulene. The permanent dipole moments of vibronic states of S_0, S_1 and S_2 are known to be sufficiently different that relatively small dc fields cause readily observable pseudo-Stark splittings of the spectral lines [11].

In the following section we will briefly review the theoretical results of our earlier paper which dealt with the microscopic form of $\chi^{(2)}$ in a three-level system, and extend the model to include first-order Stark shifts induced by a static electric field. This will allow us to apply the $\chi^{(2)}$ techniques to mixed-crystal systems with a centrosymmetric host material. Section 3 gives a detailed description of experimental apparatus and procedure. The results are presented in section 4 and discussed in section 5.

2. Theory of resonant sum- and difference-frequency generation

In the weak-field limit, the intensity of the non-linear coherent signal for sum- or difference-frequency generation is given by

$$I = \text{const.} \left| \chi_R^{(2)} + \chi_{NR}^{(2)} \right|^2 I_1 I_2. \tag{1}$$

I_1 and I_2 are the intensities of the two ingoing interacting beams, and $\chi_R^{(2)}$ and $\chi_{NR}^{(2)}$ are the resonant and the non-resonant contributions to the second-order susceptibility. For a fully resonant three-level system the resonant susceptibilities $\chi_{SUM}^{(2)}$ and $\chi_{DIF}^{(2)}$ are [2]

$$\chi_{SUM}^{(2)} = \frac{\mu_{01}^{(1)} \mu_{12}^{(2)} \mu_{20}^{(3)}}{(\omega_{10} - \omega_1 + i\Gamma_{01})[\omega_{20} - (\omega_1 + \omega_2) + i\Gamma_{02}]} , \tag{2}$$

$$\chi_{DIF}^{(2)} = \frac{\mu_{20}^{(2)} \mu_{01}^{(1)} \mu_{12}^{(3)}}{(\omega_{10} - \omega_1 + i\Gamma_{01})(\omega_{20} - \omega_2 - i\Gamma_{02})} \left(1 + \frac{i(\Gamma_{12} - \Gamma_{01} - \Gamma_{02})}{[\omega_{21} - (\omega_2 - \omega_1) - i\Gamma_{12}]} \right). \tag{3}$$

The level scheme and numbering of frequencies are given in fig. 1. The transition dipoles are denoted μ_{ij}, with the superscript denoting the corresponding field component. The ω_{ij} are the transition frequencies
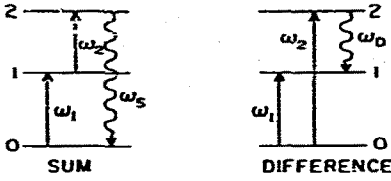
$(E_i - E_j)/h$ of the system, and the $\Gamma_{ij} = \Gamma_{ji}$ the phase relaxation parameters associated with each level pair. These susceptibilities describe a single molecule or an ensemble of identical non-interacting systems. These formulas are, therefore, appropriate for dilute mixed-crystal systems with only one orientational site per unit cell. If more than one site and orientation exist, $\chi^{(2)}$ has to be averaged accordingly.

An interesting situation is presented by mixed crystals with a centrosymmetric host material. The non-centrosymmetric guest can enter each site with two orientations generating two sublattices, k, related by a center of symmetry. Although each sublattice may have a strong second-order susceptibility, the contributions of both sublattices will cancel out. In a static electric field, however, each level is shifted by $\mu_i \cdot E_{dc}$ and the sublattices are no longer equivalent. With the abbreviation $\Delta_{ij} = (\mu_i - \mu_j) \cdot E$ the susceptibilities are given by

$$\chi^{(2)}_{SUM} = \sum_{k=1,2} \frac{(-1)^k \mu^{(1)}_{01} \mu^{(2)}_{12} \mu^{(3)}_{20}}{\left[\omega_{10} - (-1)^k \Delta_{10} - \omega_1 + i\Gamma_{10}\right]\left[\omega_{20} + (-1)^k \Delta_{20} - (\omega_1 + \omega_2) + i\Gamma_{20}\right]},$$ (4)

$$\chi^{(2)}_{DIF} = \sum_{k=1,2} \frac{(-1)^k \mu^{(2)}_{10} \mu^{(1)}_{01} \mu^{(3)}_{12}}{\left[\omega_{10} + (-1)^k \Delta_{10} - \omega_1 + i\Gamma_{10}\right]\left[\omega_{20} + (-1)^k \Delta_{20} - \omega_2 - i\Gamma_{20}\right]}$$

$$\times \left(1 + \frac{i(\Gamma_{21} - \Gamma_{20} - \Gamma_{20})}{\left[\omega_{21} + (-1)^k \Delta_{21} - (\omega_2 - \omega_1) - i\Gamma_{21}\right]}\right).$$ (5)
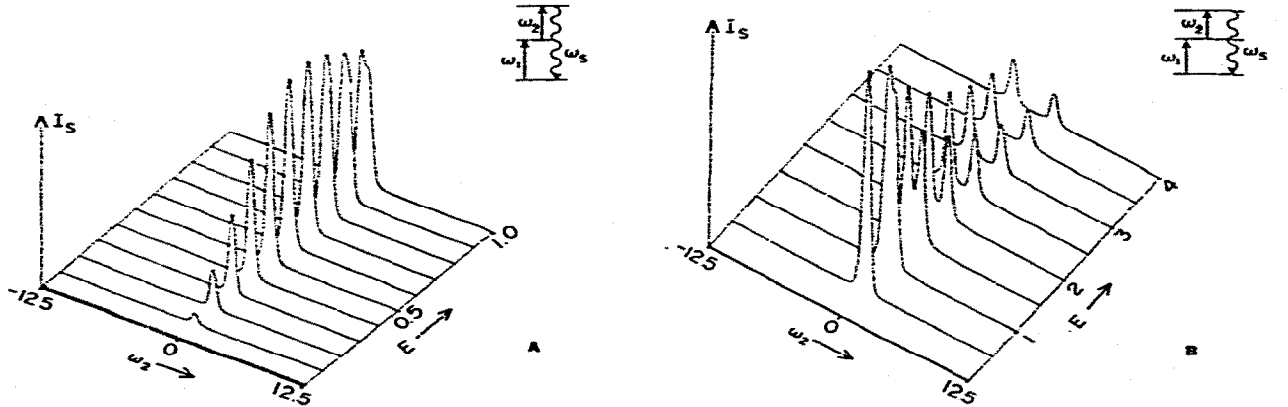

Fig. 2. Simulated lineshape of sum-frequency generation spectra for increasing strength of the static field E_{dc}. The system is modeled by the parameter values: $\Gamma_{01} = 0.9$, $\Gamma_{02} = 10^{-4}$, $b = 0.27$, $\alpha = 0.9$ (in cm^{-1}), which have been derived from ref. [12] with the assumption of full correlation between the inhomogeneous distributions of S_1 and S_2. The dipole-moment change is taken to be 1.1 D for $S_0 \rightarrow S_1$ and 1.0 D for $S_0 \rightarrow S_2$ (see ref. [11]). (A) and (B) indicate effects at low and high dc field respectively. The units of the static field are chosen so that $E_{dc} = 1$ splits the $S_0 \rightarrow S_2$ transition by 1 cm^{-1}. For all lines ω_1 was kept fixed but slightly detuned from the ω_{01} resonance ($d = 0.1$ cm^{-1}) resulting in asymmetrical lineshapes.

The expected lineshapes in sum-frequency and difference-frequency generation as a function of the static electric field are simulated in fig. 2. With low field strength, and ω_2 tuned, a resonance line is generated which has a width narrower than expected for the ω_{02} resonance. The lineshape is non-lorentzian having width $0.64\Gamma_{02}$ [a]. This signal quickly increases in intensity with increasing field strength without significant broadening. When the Stark shift becomes of the order of the linewidth, broadening and later splitting of the signal occurs. The absolute intensity of both resulting resonances drops with further increasing static-field strength, since the intermediate level will be shifted increasingly out of resonance with fixed frequency ω_1. Since we chose ω_1 not exactly at the center of the ω_{10} transition, the double-resonance picture is slightly asymmetric.

A further average is required if some levels are inhomogeneously broadened. The inhomogeneous distribution is modelled here as a static distribution of transition frequencies, with complete correlation between the distribution of the ω_{01} and ω_{02} transition frequencies. Each molecule is characterized by a parameter x indicating the energy shift from the center frequencies ω_{01}^0 and ω_{02}^0:

$$\omega_{01} = \omega_{01}^0 + x, \qquad \omega_{02} = \omega_{02}^0 + \alpha x. \tag{6}$$

Insertion of eq. (6) into eqs. (4) and (5) gives $\chi(x)$ which has to be averaged. This can be accomplished by expanding $\chi(x)$ in partial fractions:

$$\chi(x) = \sum_j c_j (x - p_j)^{-1}. \tag{7}$$

Averaging with a lorentzian distribution function with width b yields

$$\langle x \rangle_L = -\sum_j c_j s_j (ib + s_j p_j)^{-1}. \tag{8}$$

where $s_j = \text{sign}(\text{Im } p_j)$. The average with a gaussian of the same width is

$$\langle x \rangle_G = (i/b)(\pi/2)^{1/2} \sum_j c_j s_j w(s_j p_j / 2^{1/2} b). \tag{9}$$

where $w(z)$ is the complex error function. For the sum-frequency susceptibility the poles p_j and coefficients c_j are

$$p_1 = \omega_{10}^0 + (-1)^k \Delta_{10} - \omega_1 + i\Gamma_{01}, \qquad p_2 = \left[\omega_{20}^0 + (-1)^k \Delta_{20} - (\omega_1 + \omega_2) + i\Gamma_{02} \right]/\alpha.$$

$$c_1 = (-1)^k \mu_{01}^{(1)} \mu_{12}^{(2)} \mu_{20}^{(3)} / (p_1 - p_2) \cdot \alpha, \qquad c_2 = -c_1. \tag{10}$$

Of course, the poles and coefficients occur in pairs with $k = 1, 2$. For difference frequency the additional results are

$$p_2 = \left[\omega_{20}^0 + (-1)^k \Delta_{20} - \omega_2 - i\Gamma_{20} \right]/\alpha, \qquad p_3 = \left[\omega_{21}^0 + (-1)^k \Delta_{21} - (\omega_2 - \omega_1) - i\Gamma_{12} \right]/\beta.$$

$$c_1 = \left[(-1)^k \bar{\mu}/\alpha (p_1 - p_2) \right] \left[1 - i\Gamma'/\beta (p_1 - p_3) \right].$$

$$c_2 = \left[(-1)^k \bar{\mu}/\alpha (p_2 - p_1) \right] \left[1 - i\Gamma'/\beta (p_2 - p_3) \right], \qquad c_3 = -(c_1 + c_2). \tag{11}$$

with $\bar{\mu} = \mu_{20}^{(2)} \mu_{01}^{(1)} \mu_{12}^{(3)}$ and $\Gamma' = \Gamma_{12} - \Gamma_{01} - \Gamma_{02}$.

From these and corresponding simulations for difference-frequency generation, we expect that spectra taken with relatively small static-field strengths will provide information equivalent to that obtainable from

[a] For $\Gamma_{02} \ll \Gamma_{01}$, or ω_1 detuned from resonance, the expansion of expression (4) in powers of the dc-field strength yields, in lowest order, a resonance susceptibility: $\chi \propto E_{dc}[\omega_{20} - (\omega_1 + \omega_2) + i\Gamma_{02}]^{-2}$.

a single sublattice. The use of a centrosymmetric host molecule has the advantage that the non-resonant part $\chi_{NR}^{(2)}$ of the susceptibility can be neglected, since much higher field strengths than used in this work would be necessary to induce frequency mixing in a centrosymmetric crystal composed of molecules which have no dipole moments.

3. Experimental

Our sample consisted of a naphthalene single crystal doped with $\approx 10^{-5}$ mole/mole azulene. The levels chosen as the three-level system 0, 1, 2 are the vibrationless levels of S_0, S_1 (14651 cm^{-1}) and S_2 (28048 cm^{-1}). The frequencies of the transitions $0 \rightarrow 1$, $0 \rightarrow 2$ as well as that of the $1 \rightarrow 2$ transition can be generated with dye lasers. The experimental arrangement is schematically shown in fig. 3. Two dye lasers were simultaneously pumped by the frequency-doubled output of a Nd:YAG laser (Quanta Ray). The first laser (DL1, nile blue) operates at 6825 Å resonant with the $S_0 \rightarrow S_1$ transition. For the sum-frequency experiment the second dye laser (DL2, LDS 750, Exciton) operates at 7464 Å, while for the difference-frequency experiment it is tuned to 7131 Å, doubled, and the fundamental removed with a CuSO$_4$ solution filter (F$_2$). Fluorescence of DL1 which interferes with the detection of the difference-frequency signal was removed by triple prisms (P) in combination with an aperture (A) as well as a short-pass (7000 Å) interference filter (F$_1$). The parallel beams were focused (L$_1$, $f = 400$ mm) into the sample immersed in liquid helium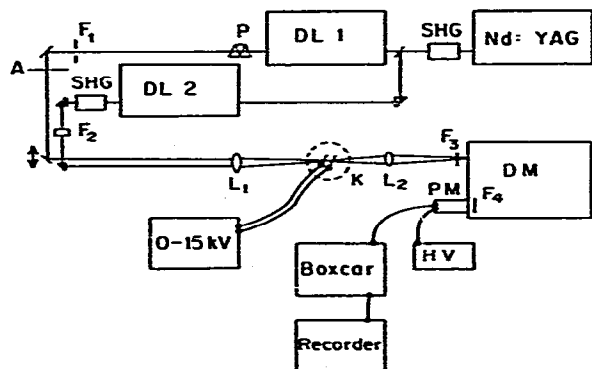. The forward going light containing the signal was brought into the entrance slit of a double monochromator (Spex 1401). The laser light was blocked with appropriate filters: for sum-frequency detection F$_3$ = Corning #9863 and a CuSO$_4$ solution filter; for difference-frequency detection F$_4$ = Schott RC 715. The non-linearly generated photons were detected with a red-sensitive photomultiplier (RCA 31034) and the signal processed with a boxcar integrator (PAR 162/164).

Both dye lasers had linewidths of ≈ 1 cm^{-1} when operated without intracavity etalons. For high-resolution spectra intracavity etalons were inserted reducing the linewidth to 0.1 cm^{-1}. In this case scanning was achieved by pressure tuning with N$_2$ gas.

The sample was placed between electrodes to which up to 15 kV could be applied by a high-voltage power supply. Two arrangements have been used (fig. 4): In the first, the crystal was placed between copper electrodes in such a way that the static electric field lay in the *ab* cleavage plane of the crystal which was normal to the incident laser beams (fig. 4a). The second arrangement used transparent electrodes holding a thin slice of the crystal which again was cut along the cleavage plane. Thus the static electric field was perpendicular to *ab* in this case. The second arrangement allowed the use of thinner crystals, and consequently the application of higher Stark fields. In addition, Stark splittings are 5 times larger with

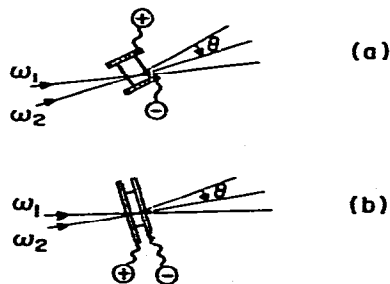Fig. 3. Schematic of apparatus used for sum- and difference-frequency generation.

Fig. 4. Two Stark-cell configurations used in measurements as discussed in text.

this field orientation compared with the field along the crystallographic *b* axis, and $2^{1/2}$ times larger than for the *a*-axis orientation of the field [11]. It also allowed a larger variation of θ, the angle between the beam propagation and the c' axis of the crystal. In the first arrangement the copper electrodes obscure the crystal for larger values of θ. Fine tuning of θ is essential to achieve proper phase-matching.

The crystal *b* axis of naphthalene is parallel to the optical principal axis *y*, while the *ac* plane contains the principal axes *x*, *z* and the two optical axes. Phase-matching can therefore be achieved with all beams propagating in the *ac* plane when the red beams (resonant with $S_0 \rightarrow S_2$ and $S_1 \rightarrow S_2$) are polarized parallel to *b* and the UV is polarized perpendicular to *b*. Tuning the angle θ will change the refractive index for the UV beam only. We estimated $\theta \approx 30°$ for collinear beams.

The values used for permanent dipole moments (Stark shifts), homogeneous and inhomogeneous linewidth in the simulation are given in the caption to fig. 2. All the observations were carefully compared with numerical simulations, using these parameters, based on eqs. (7) or (8).

4. Results and discussion

4.1. Sum-frequency spectra

Phase-matched sum-frequency spectra were easily obtained in both crystal orientations. Fig. 5 shows the result of scans of ω_2 with ω_1 fixed on resonance for increasing strength of the static electric field. The spectra were essentially the same when the fixed and the scanned frequency were switched. The linewidths correspond to the (inhomogeneous) width of the ω_{02} transition, in complete agreement with expectation: When ω_2 is scanned we expect the same line as for the $S_0 \rightarrow S_2$ absorption spectrum, while with ω_1 scanned this spectrum is multiplied with the $S_0 \rightarrow S_1$ spectrum. Since the latter is much broader, nearly the same lines result in both cases. The peak intensity first rises quadratically with the static-field strength, but then for larger fields the increase becomes linear (fig. 6). With even larger Stark effects, obtainable with the static field along the c' axis, splitting of the signal is observed indicating complete separation of the two sublattices (fig. 7). The observed pattern is in quite good agreement with the simulation of fig. 2.

The effect of the broader ω_{01} resonance was most conveniently demonstrated in an indirect way. Scans of ω_2 were repeated for a fixed dc field with varying detuning of ω_1 from ω_{01}. The sum-
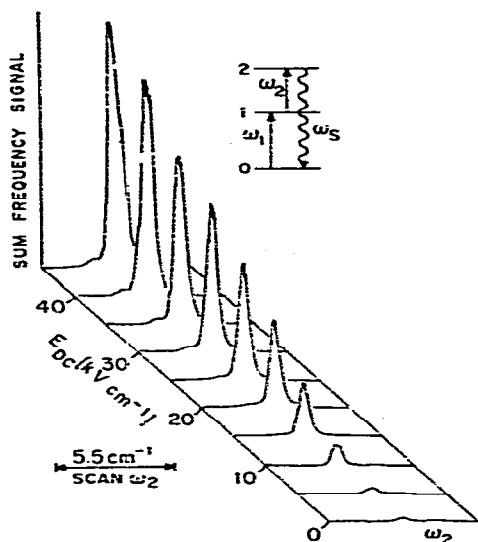

Fig. 5. Sum-frequency generated signal for increasing strength of the dc field (in *ab* orientation as shown in fig. 4a). ω_2 is pressure scanned, ω_1 is fixed on the resonance ω_{01}.
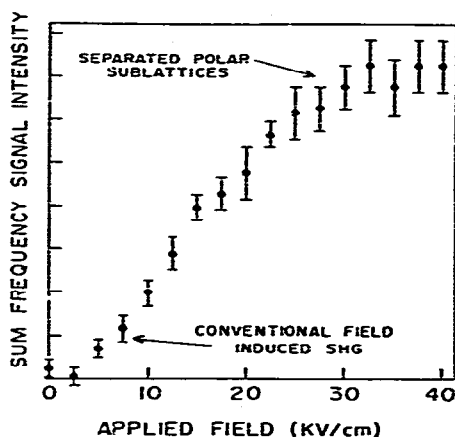

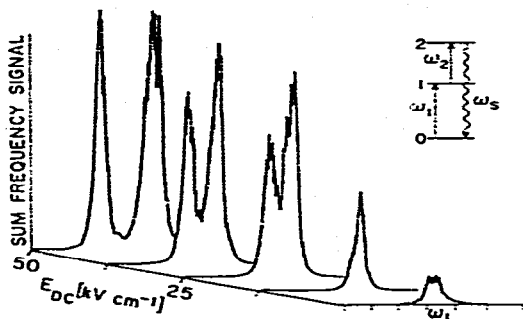Fig. 6. Variation of peak sum-frequency signal with dc-field strength, field in *ab* orientation, both laser frequencies fixed.

Fig. 7. Sum-frequency generation spectra for increasing dc-field strength in c' direction. ω_2 pressure scanned. ω_1 fixed on the ω_{01} resonance.

frequency resonance was detected at each detuning, and its peak intensity plotted against the detuning revealed the ω_{01} resonance (fig. 8). The agreement with the simulation is again satisfactory.

A direct observation of the ω_{31} resonance also proved possible. With ω_2 detuned from the ω_{12} resonance, a scan of ω_1 should realize the resonance conditions $\omega_{01} + \omega_1 = 0$ and $\omega_{02} + \omega_1 + \omega_2 = 0$ consecutively. Consequently two resonances should appear separated by the detuning of ω_2. The result of this experiment is shown in fig. 9. On the wing of the ω_{02} resonance a second resonance
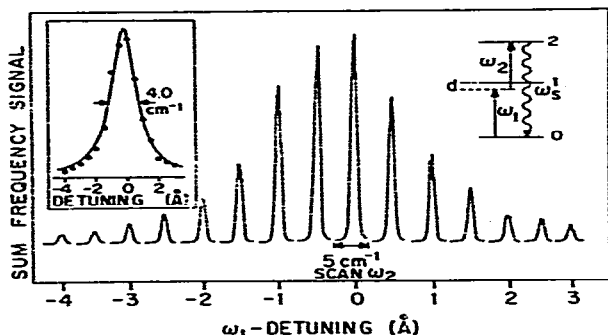

Fig. 8. Indirect observation of the ω_{01} resonance in sum-frequency generation. ω_2 is scanned with ω_1 fixed with detuning d from the ω_{01} resonance. One line is observed for each detuning. The peak heights are plotted versus the detuning d in the inset revealing the ω_{01} resonance. The full line in the inset is a fitted lorentzian. Both lasers were operated without intracavity etalons, accounting for the linewidths being greater than Γ_{01}.
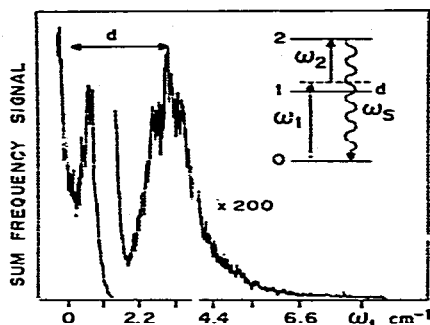

Fig. 9. Direct observation of the ω_{01} resonance for sum-frequency generation. ω_1 is pressure scanned while ω_2 is fixed detuned ≈ 3 cm^{-1} below the $S_1 \to S_2$ resonance. The lower-energy member of the ω_{02}-resonance doublet is seen at the left while the high-energy member falls just outside the pressure scan range. At a detuning d to lower energies (corresponding to $\omega_1 = \omega_{10}$) a weak resonance with larger width is seen. The width, however, is smaller than $2\Gamma_{01}$ (≈ 1.5 cm^{-1}) indicating that fields generated in the two sublattices interfere destructively at the wings.

with width Γ_{01} and much lower intensity appears. The simulation using eq. (4) gives the same pattern but overestimates the intensity of the second band. This discrepancy is thought to result from the neglect of the changes in the phase-matching/absorption factor over the scan range.

4.2. Difference-frequency spectra

In the absence of pure dephasing the difference-frequency susceptibility is predicted to show the same resonances as the sum-frequency susceptibility, but with the two frequency scans completely decoupled. This means that when either ω_1 or ω_2 is scanned the difference mixing lineshape should follow the absorption spectrum of S_1 or S_2 respectively.

Signal levels in difference generation were much lower than for sum generation since the ω_2 beam required to be frequency doubled. Signals were obtained using the transparent electrode arrangement only when the dc field was along c'. Phase-matching was found to be very critical.

The difference spectra with ω_2 scanned for increasing dc-field strength are given in fig. 10. They closely resemble the corresponding spectra in sum-frequency generation (fig. 7). The linewidths
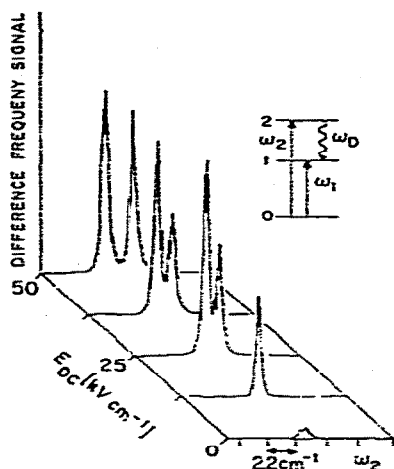
Fig. 10. Difference-frequency generation spectra for increasing dc-field strength in c' direction. ω_2 is pressure scanned, ω_1 fixed on the ω_{01} resonance.

and Stark splittings in the conventional absorption spectra of the $S_0 \rightarrow S_2$ transition taken with the same ω_2 scan are given in fig. 11.

The ω_{01} resonance was measured indirectly using the method of scanning ω_2 for various detunings of ω_1. Fig. 12 shows the experimental result which agrees well with the theoretical predictions. The decoupling of the ω_1 and ω_2 scan makes the direct observation of the ω_{01} resonance much easier than in the sum-frequency case.

Pressure scans of ω_1 for increasing dc-field strength are shown in fig. 13. The lineshapes are
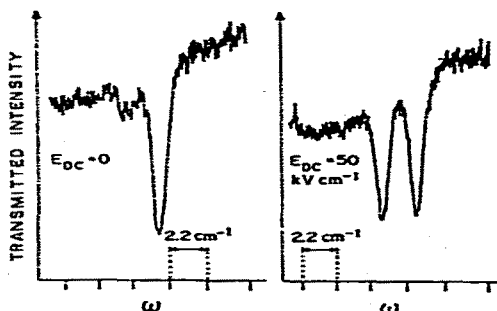

Fig. 11. Conventional transmission spectra of the $0 \rightarrow 2$ vibrationless transition of azulene. The beam geometry is the same as used for difference-frequency generation.
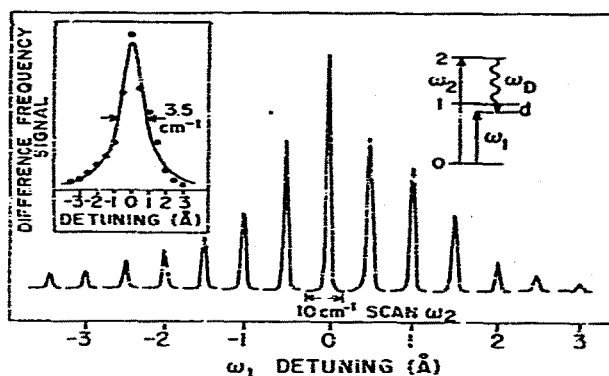

Fig. 12. Indirect observation of the ω_{01} resonance in difference-frequency mixing. The same technique as in fig. 8 has been used.

unsymmetrical due to the non-linear scan (see etalon markers). The applied Stark field was not strong enough to split the S_1 transition sufficiently in this case.

4.3. The DICE resonance

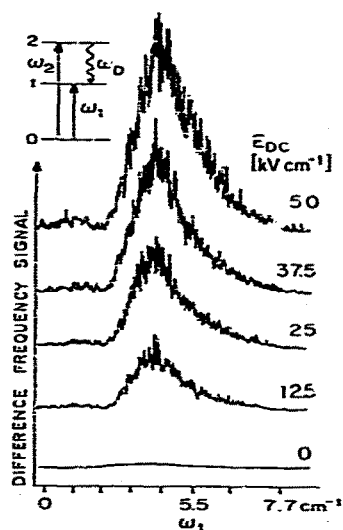The only resonance predicted for the fully resonant sum and difference spectroscopies that has

Fig. 13. Pressure scan of the ω_{01} resonance in difference-frequency generation for increasing strength of the dc field.

not yet been found is the extra resonance in difference-frequency generation induced by pure dephasing. The resonance is related to a similar phenomenon in CSRS spectroscopy where it has been both predicted and observed for solids [4,5] and gaseous systems [6,7]. In the gas phase the pure dephasing may be induced by collisions, while in solids raising the temperature enables pure dephasing processes to occur.

In difference-frequency spectroscopy the DICE (dephasing-induced coherent emission) resonance depends on Γ' being equal to zero, and it is the ω_{12} resonance (see eq. (3)). It should appear separated from the other resonances when one laser is kept fixed but detuned from resonance, while the second laser is scanned. For example with ω_1 detuned from ω_{01} by an amount d, a scan of ω_2 will show the ordinary resonance at $\omega_2 = \omega_{20}$ and the DICE resonance at $\omega_2 = \omega_{20} + d$, corresponding to $\omega_{21} = \omega_2 - \omega_1$. This resonance will shift with varying detuning d, and increase in intensity with increasing temperature due to the increase in Γ'.

No trace of the DICE resonance could be found at 4.2 K suggesting that this temperature is still too low to introduce sufficient pure dephasing. The Stark cell was therefore modified and incorporated into a temperature-controlled cryostat allowing temperatures upwards of 5 K. Cooling was achieved by helium exchange gas, whose pressure had been set to ≈ 1 atm instead of the recommended value of 1 Torr to prevent discharges in the Stark apparatus. Although only low static fields ($< 20\,000$ V cm^{-1}) could be applied, the difference-frequency effect was readily observed. However, raising of the temperature resulted only in decreasing intensity of the familiar $\omega_2 = \omega_{20}$ resonance until above 20 K this resonance dropped to the noise level. No DICE resonance was found.

To gain more insight into this situation spectra were calculated with the parameter set of fig. 2. The pure dephasing contribution to all linewidths was assumed to be equal. The resulting lineshapes indicate that the expected DICE resonance is more than three orders of magnitude weaker than the main resonance and should result in a small inflexion only. Obviously the signal-to-noise ratio in our experiment is too low to allow such an observation. Azulene, then, appears to be an unfavorable example for this particular effect.

4.4. Hysteresis effect

With the laser beams passing through the transparent electrodes a hysteresis effect was observed. When the voltage was switched off, the Stark-induced $\chi^{(2)}$ effect disappeared only slowly over several minutes. On the other hand the Stark effect responded immediately to changes in the applied voltage when the opaque copper electrodes were used. All plots of I versus E_{dc} were therefore derived from data obtained in the latter configuration.

This hysteresis effect can be explained on the assumption that electrons from the electrode are injected into the crystal surface as a result of the intense laser field. Due to the high electric resistance of the organic material this should have only minor effects on the field inside the crystal, but the capacitor will discharge slowly, thereby accounting for the continuation of the $\chi^{(2)}$ signal in the absence of the applied field. Such space-charge effects may be quite useful in themselves for creating second-order optical phenomena in otherwise centrosymmetric organic solids.

4.5. Line narrowing

The ω_{02} and ω_{01} resonances appear very similar in the sum- and difference-frequency spectra, although complementary line-narrowing properties are predicted for both processes. At first sight this seems to indicate that no correlation exists between the inhomogeneous distributions of the two excited states involved. Such a conclusion is not yet justified. All the observed lineshapes are in accord with a model of full correlation between the various levels.

We showed previously that the widths of some of the resonances in sum- and difference-frequency generation could be modified from those expected from the energy spread caused by the inhomogeneous distribution. The homogeneous width is expected to dominate the lineshapes in difference-frequency generation in the case that the correlation factor joining the $0 \to 1$ and $0 \to 2$ distributions is unity [2]. This is referred to as the fully correlated case. The expected width in such a case, assuming ω_2 is scanned, is $\bar{\Gamma} = \alpha \Gamma_{12} + (1 - \alpha)\Gamma_{02}$

where α, as before, is the ratio of the inhomogeneous widths for the $0 \to 2$ and $0 \to 1$ transitions. In the absence of correlation the width is expected to be $\Gamma_{02} + \alpha\sigma$ which is the inhomogeneous linewidth of the $0 \to 2$ transition. For azulene we have $\Gamma_{02} \ll \sigma < \Gamma_{01}$, while $\bar{\Gamma} = \alpha\Gamma_{bc}$, so that the purely homogeneous contribution to the non-linear spectral width is wider than the inhomogeneous part. When ω_1 is scanned the situation is comparable: The uncorrelated width is expected to be $\Gamma_{01} + \sigma$, whereas the homogeneous width in the fully correlated system should have the width Γ_{12}. However, in the absence of pure dephasing $\Gamma_{21} = \Gamma_{01}$ and $\Gamma_{01} > \sigma$. Hence the correlations within the homogeneous distributions have only a slight effect on the observed linewidths in this case. In order to demonstrate line-narrowing effects more dramatically the inhomogeneous part of the linewidth should dominate all the other contributions.

5. Conclusions

The predicted spectroscopic properties of fully resonant sum- and difference-frequency generation have been examined in a doped organic molecular crystal at low temperatures. The host crystal was centrosymmetric, and the macroscopic susceptibility $\chi^{(2)}$ was induced by Stark-shifting the sublattices of the polar guest molecules. This Stark-effect technique has two advantages: It extends the applicability to centrosymmetric crystals and it eliminates interferences with the non-resonant susceptibility of the host material. The latter effect caused serious problems in preliminary experiments using acenaphthene as the host material. Although non-resonant, the high concentration of the host completely outweighted the resonant contribution from the dilute guest and the signal was dominated by the background.

All resonances of $\chi^{(2)}$ expected in a system with negligible pure dephasing could be found. In the system studied here the dephasing-induced (DICE) resonance is expected to be very weak, and at the high temperatures necessary to induce the effect the total intensity of the coherent signal drops rapidly below the detection limit. Better conditions

are expected to exist in systems with a longer lifetime of the first excited level.

The susceptibilities for sum- and difference-frequency spectroscopy have complementary line-narrowing capabilities. Any system with sufficient correlation of the inhomogeneous distributions should give line-narrowed spectra in one or both processes. For the effect to be readily observable the inhomogeneous distribution should dominate both linewidths.

An interesting aspect of the present work concerns the field dependence of the signal which is not quadratic like conventional electric-field-incued $\chi^{(2)}$ processes. The signal can be caused to saturate at relatively low fields. This result is seen in figs. 3, 6 and 10. The saturation effect arises because a separated non-centrosymmetric sublattice is responsible for the non-linear signal above a certain dc-field strength where $E\Delta\mu$ exceeds the transition linewidth.

This new technique is neither restricted to crystals nor to the use of visible dye lasers. On the contrary, we expect it to be especially useful in the study of vibrational relaxation processes with one of the lasers being in resonance with an infrared-allowed transition of the ground or the excited state. Phase-matching should be less critical under such conditions. Other applications involve surface studies and glasses, where phase-matching is also readily achieved in most situations.

References

[1] R.M. Hochstrasser and H.P. Trommsdorff, Accounts Chem. Res. 16 (1983) 376.
[2] B. Dick and R.M. Hochstrasser, J. Chem. Phys. 78 (1983) 3398.
[3] N. Bloembergen, H. Lotem and R.T. Lynch Jr., Indian J. Pure Appl. Phys. 16A (1977) 15.
[4] J.R. Andrews, R.M. Hochstrasser and H.P. Trommsdorff, Chem. Phys. 62 (1981) 87.
[5] J.R. Andrews and R.M. Hochstrasser, Chem. Phys. Letters 82 (1981) 381; 83 (1981) 427.
[6] Y. Prior, A.R. Bodgan, M. Dagenais and N. Bloembergen, Phys. Rev. Letters 46 (1981) 111.
[7] A.R. Bodgan, Y. Prior and N. Bloembergen, Opt. Letters 6 (1981) 82.
[8] B. Dick and R.M. Hochstrasser, Phys. Rev. Letters 51 (1983) 2111.

[9] J.W. Sidman and M.S. McClure, J. Chem. Phys. 24 (1956) 757.

[10] A.R. Lacy, R.G. Budy, G. Frank and I.G. Ross, J. Chem. Phys. 47 (1967) 2159.

[11] R.M. Hochstrasser and L.J. Noe, J. Chem. Phys. 50 (1969) 1684.

[12] R.M. Hochstrasser and T.Y. Li, J. Mol. Spectry. 41 (1972) 297.

[13] G.J. Small and S. Kusserow, J. Chem. Phys. 60 (1974) 1558.

[14] J.M. Friedman and R.M. Hochstrasser, Chem. Phys. 6 (1974) 145.

[15] R.M. Hochstrasser and C.A. Nyi, J. Chem. Phys. 70 (1979) 1112.

[16] R.M. Hochstrasser, Accounts Chem. Res. 6 (1973) 263.